

Image-based near-surface modeling for statics corrections

Öz Yilmaz¹

Abstract

The near-surface is usually defined as the depth interval below the topography, composed of a low-velocity soil column and weathered rock layer. In contrast with the near-surface, the subsurface is composed of relatively higher velocity rock layers. This means that the interface between the near-surface and the subsurface often gives rise to a strong shallow reflection. The image-based method described in this paper makes use of the strong reflection at the base of the near-surface to estimate a model for the near-surface for statics corrections. The method is based on construction of constant-velocity migration volume by prestack time migration of shot records. The near-surface rms velocities associated with the strong reflector at the base of the near-surface are picked from the semblance spectra to create the near-surface rms velocity field. This laterally varying, but vertically invariant, velocity field actually is equivalent to the near-surface interval velocity field, which can be used to perform prestack depth migration of shot records to obtain a shallow seismic image of the near-surface. Finally, the depth horizon associated with the base of the near-surface is delineated from this shallow seismic image. The image-based near-surface model is formed by combining this depth horizon with the interval velocity field. This image-based model for the near-surface yields essentially the same statics that one calculates from a more complicated model for the near-surface that may be estimated from inversion methods.

Summary

In exploration seismology, the most common type of the near-surface is defined as the depth interval below the topography, composed of a low-velocity, unconsolidated, heterogeneous soil column and weathered rock layer. As such, raypaths are close to vertical incidence within the near-surface — a requirement for statics corrections to be acceptable. This definition of the near-surface does not apply to the case of a rock outcrop. Hence, if it is *near the*

surface, it is not always *the near-surface* within the context of the definition above. In contrast with the near-surface defined above, the *subsurface* is composed of relatively higher velocity, consolidated rock layers. As such, the interface between the near-surface and the subsurface often gives rise to a strong shallow reflection.

Aside from the old methods of uphole surveys and shallow seismic surveys, the methods for near-surface modeling include traveltimes inversion (Zhou et al., 1992; Zhang and Toksöz, 1998), waveform inversion (Liu and Zhang, 2014), joint inversion of seismic and gravity (Colombo et al., 2013; Zhou et al., 2014), joint inversion of seismic and electromagnetic data (Abubakar et al., 2012; Ogunbo and Zhang, 2014; Marquis et al., 2016), joint inversion of seismic and resistivity data (Zhang and Morgan, 1997; Gallardo and Meju, 2004), and hybrid inversion of traveltimes and waveform (Zhang and Chen, 2014; Liu and Zhang, 2015) (Figure 1).

In a previous *TLE* paper (Yilmaz, 2013), I described an image-based method, which makes use of the strong reflection at the base of the near-surface, to estimate a model for the near-surface for statics corrections. The method (termed *i-stats* for brevity) is based on prestack depth migration of shot records from a floating datum that closely resembles surface topography using a range of near-surface velocities. The resulting depth images form an image volume, which can then be interpreted to pick the reflector associated with the base of the near-surface and to pick the velocities for the near-surface from the corresponding horizon-consistent semblance spectrum. The estimated “*equivalent-medium*” model for the near-surface comprises laterally varying velocities only, but yields essentially the same statics that one calculates from a more complicated model for the near-surface that may be estimated from inversion methods. The equivalent-medium model of the near-surface conforms to the vertical raypath assumption that underlies statics corrections. In the 2013 paper, I demonstrated the *i-stats* method to correct for the deleterious effect of near-surface anomalies associated with sand dunes, shallow anhydrites, and glacial tills on subsurface reflections.

In this paper, I present a case study for the near-surface that consists of salt-filled karstic formation from the Volga Region of Western Siberia. I also describe a modification to the *i-stats* workflow so that the method can be applied to 3-D seismic data. In the new *i-stats* workflow, we create a constant-velocity migration (CVM) volume by prestack time migration of shot records. The near-surface rms velocities associated with the strong reflector at the base of the near-surface are picked from the semblance spectra to create the near-surface rms velocity field. This laterally varying, but vertically invariant, velocity field actually is equivalent to the near-surface interval velocity field, which can be used to perform prestack depth migration of shot records to obtain a shallow seismic image of the near-surface. Finally, the depth horizon associated with the base of the near-surface is delineated from this shallow seismic image.

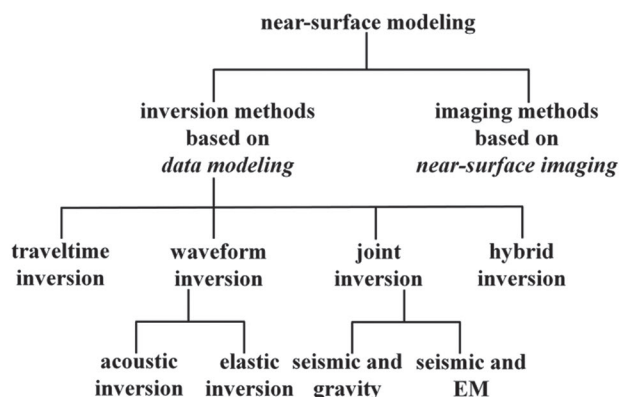


Figure 1. Methods for near-surface modeling. Traveltimes inversion currently is the most widely used method for near-surface modeling; whereas, other inversion methods are still in development stages with limited applicability to real data. In this paper, the image-based method is demonstrated by a case study.

¹GeoTomo LLC.

<http://dx.doi.org/10.1190/tle35110936.1>

The near-surface equivalent-medium model to calculate shot-receiver statics is formed by combining this depth horizon with the interval velocity field.

The near-surface

Figures 2–6 (Yilmaz, 2015) show five different cases of the near-surface model which fit the description above — the near-surface composed of a low-velocity, unconsolidated, heterogeneous soil column and weathered rock layer. The near-surface velocity-depth models shown in these figures were estimated by nonlinear traveltime tomography applied to first-arrival times picked from the shot records (Zhang and Toksöz, 1998). The seismic image in each of the five cases in Figures 2–6 exhibits a strong reflector that corresponds to the strong velocity contrast at the interface between the near-surface and the subsurface. The *i*-stats method would not be applicable if a strong reflector associated with the base of the near-surface is unidentifiable.

Shown in Figure 2 is the case of a near-surface with sand dunes in North Africa. The velocity-depth model accurately describes the anatomy of sand dunes: a low-velocity (around 500–600 m/s) cap on top of the dunes associated with dry sands, an interior with wet sands with velocity around 1500 m/s, and a root with relatively higher velocity. The vertical velocity gradient within the sand dunes is a result of gradual accumulation of wind-swept sands within a topographic obstacle. Shown in Figure 3 is the case of a near-surface above a shallow evaporite layer in the Middle East. The velocity-depth model exhibits the complexity of the shallow anhydrite layer resulting from solution collapses. Shown in Figure 4 is the case of a near-surface with glacial till comprising low-velocity material in Western Canada. Shown in Figure 5 is the case of a near-surface above a shallow salt layer from Turkey. The velocity-depth model exhibits the rugose interface at the top-salt boundary. Finally, shown in Figure 6 is the case of a near-surface above a shallow basalt layer from North Africa. The velocity-depth model exhibits the irregular interface at the top-basalt boundary. Note that in all five cases shown in Figures 2–6, the geometry of the interface that represents the boundary between the near-surface and the subsurface (represented by the red

color in the velocity-depth models) closely follows the geometry of the strong reflector observed in the shallow seismic images.

The *i*-stats case study: Data from Western Siberia

Figure 7 shows a constant-velocity stack (CVS) panel with a velocity optimum for the near-surface and a CVS panel with a velocity optimum for the subsurface. Both sections are with elevation statics applied to lower the shots and receivers from

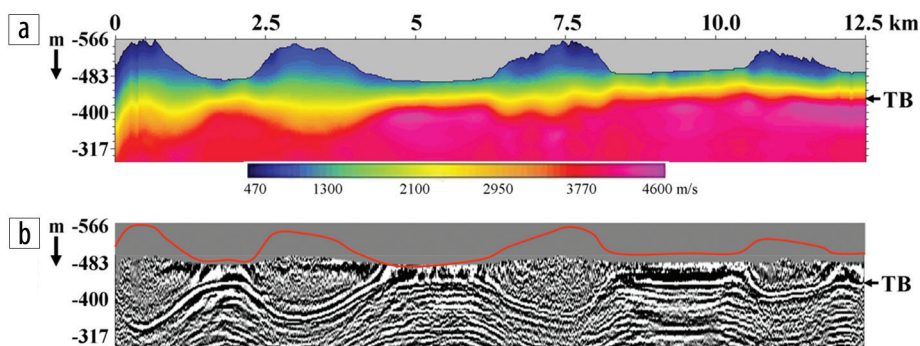


Figure 2. (a) The velocity-depth model for the near-surface with sand dunes from North Africa; (b) the corresponding shallow seismic image. TB: top-bedrock — the interface between the near-surface above and the subsurface below — represented by the strong reflector in (b) (Yilmaz, 2015).

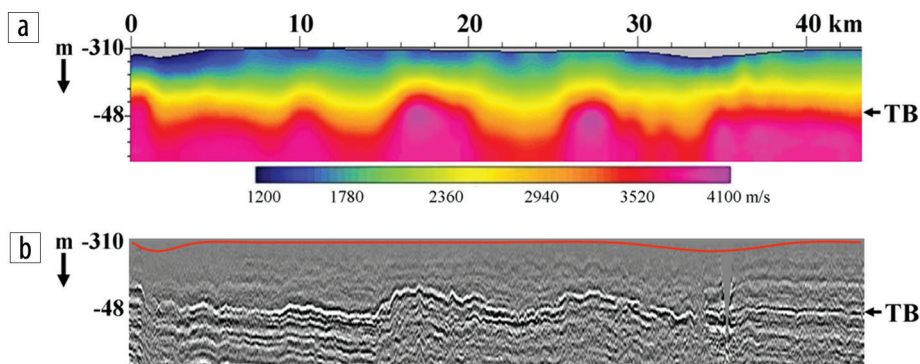


Figure 3. (a) The velocity-depth model for the near-surface above an evaporite layer with solution collapses from the Middle East; (b) the corresponding shallow seismic image. TB: top-bedrock — the interface between the near-surface above and the subsurface below — represented by the strong reflector in (b) (Yilmaz, 2015).

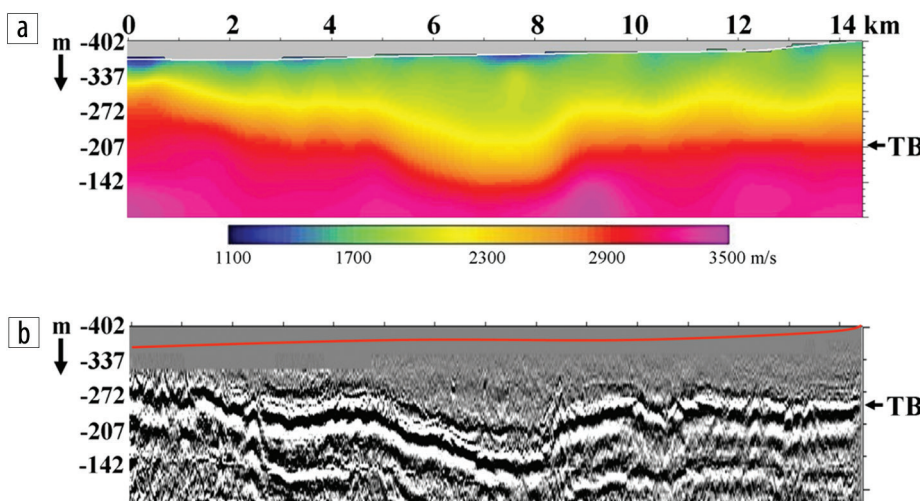


Figure 4. (a) The velocity-depth model for the near-surface with glacial till from Canada; (b) the corresponding shallow seismic image. TB: top-bedrock — the interface between the near-surface above and the subsurface below — represented by the strong reflector in (b) (Yilmaz, 2015).

topography to a floating datum followed by residual statics corrections. The salt-filled karstic formation within the near-surface, especially in the vicinity of the vertical red bar, has given rise to severe distortions in the reflector geometry within the subsurface.

Figure 8 shows the stages of the new i-stats workflow to derive the near-surface equivalent-medium model for statics corrections.

- 1) Apply elevation statics corrections to move the shots and receivers from surface topography to a floating datum that closely resembles the topographic variations with wavelengths greater than half the cable length using a velocity associated with the upper near-surface.
- 2) Apply appropriate signal processing to shot gathers tailored for shallow seismic imaging (Yilmaz, 2015). Specifically, apply a parsimonious processing sequence to minimize amplitude distortions and attain a high-resolution shallow seismic image with broadest possible signal bandwidth. In the present case, the processing sequence included trace balancing, geometric spreading correction, and time-variant spectral whitening within the 8–84 Hz passband. If surface-wave amplitudes are overwhelmingly strong at low frequencies, then you may be compelled to limit the passband to higher frequencies, such as 24–84 Hz. Additionally, to improve the shallow seismic image, if necessary, calculate and apply shot-receiver residual statics. Unlike the conventional sequence of long-wavelength statics estimation followed by residual statics estimation, the i-stats method in some cases may require reversal of this order.
- 3) Perform constant-velocity prestack time migration (CVM) of shot records from the floating datum using a range of near-surface velocities. The resulting image panels (Figure 8a) form an image volume, which is used to pick the near-surface rms velocities from the semblance spectra down to the

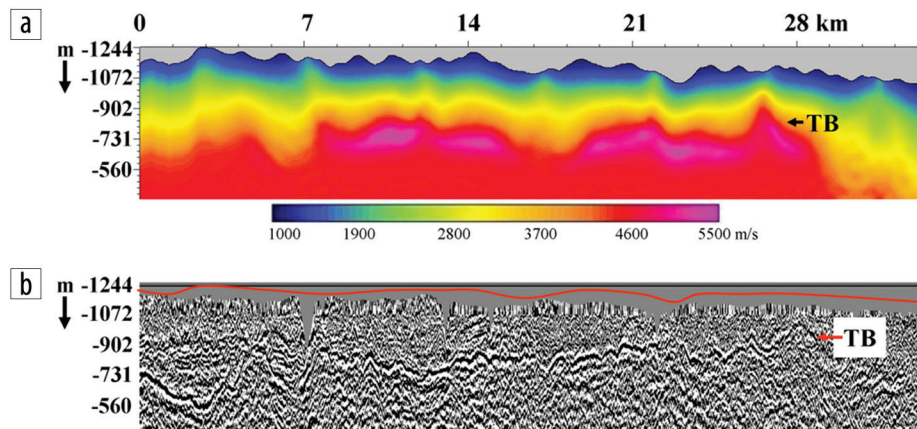


Figure 5. (a) The velocity-depth model for the near-surface above a salt layer with rugose top interface from Turkey; (b) the corresponding shallow seismic image. TB: top-bedrock — the interface between the near-surface above and the subsurface below — represented by the strong reflector in (b) (Yilmaz, 2015).

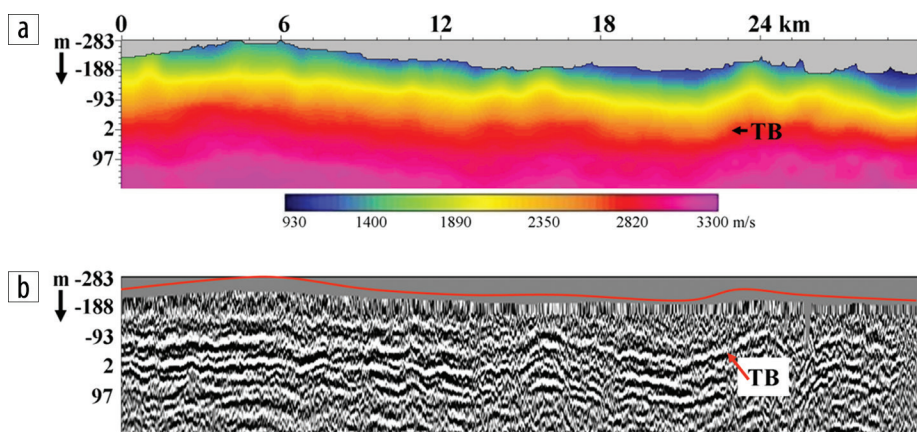


Figure 6. (a) The velocity-depth model for the near-surface above a basalt layer with rugose top interface from North Africa; (b) the corresponding shallow seismic image. TB: top-bedrock — the interface between the near-surface above and the subsurface below — represented by the strong reflector in (b) (Yilmaz, 2015).

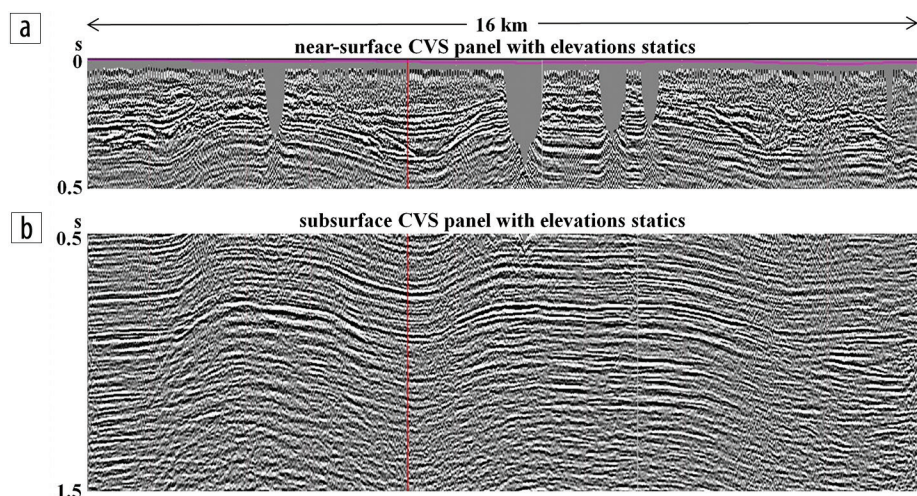


Figure 7. (a) A constant-velocity stack (CVS) panel with a velocity optimum for the near-surface, and (b) a CVS panel with a velocity optimum for the subsurface. Both sections are with elevation statics applied to lower the shots and receivers from topography to a floating datum followed by residual statics corrections. The karstic formation in the near-surface has given rise to severe distortions in the reflector geometry within the subsurface.

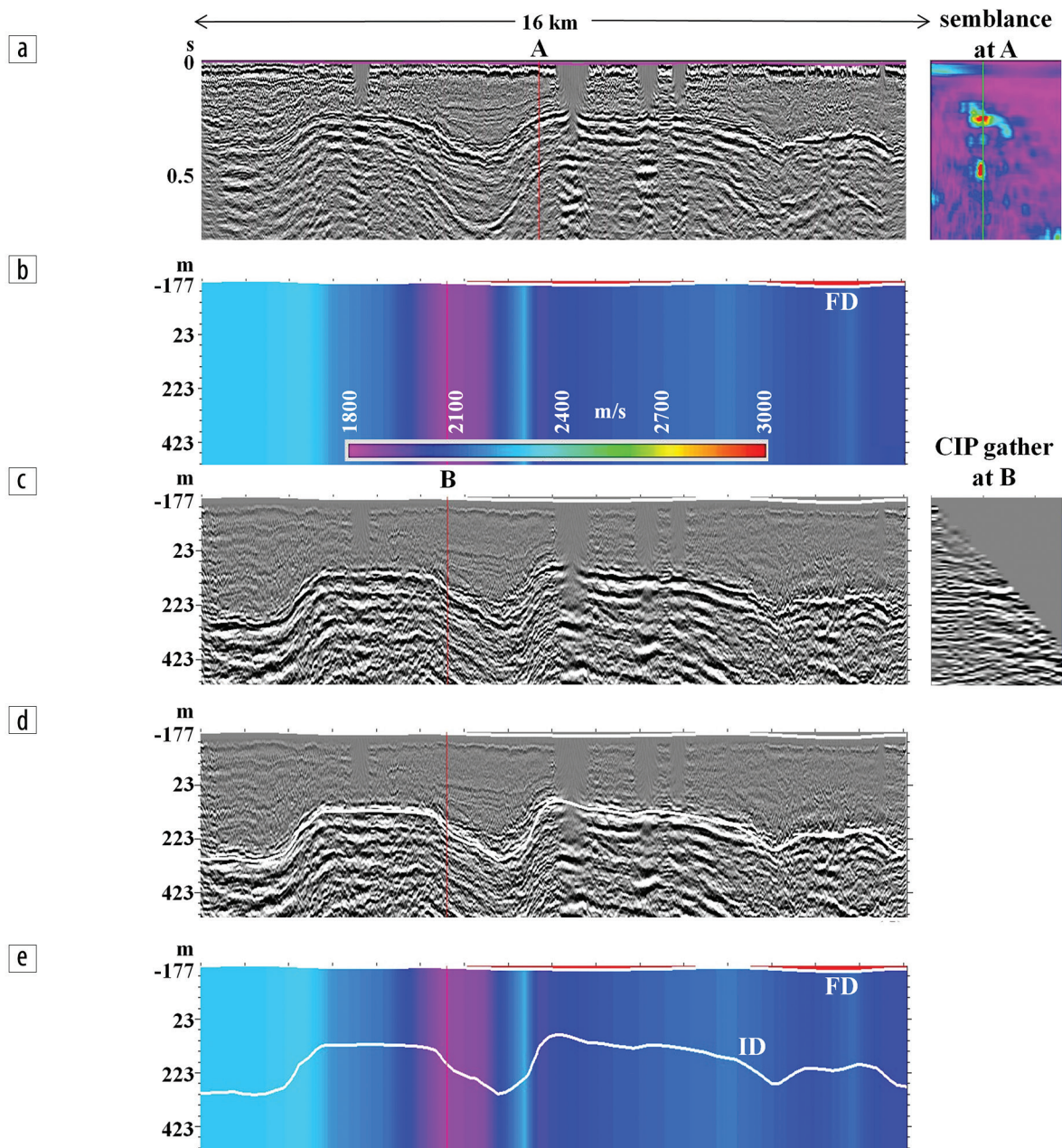


Figure 8. (a) A constant-velocity prestack time migration (CVM) panel with a velocity optimum for near-surface imaging and a semblance spectrum at location A with a velocity range 1000–3500 m/s. Note the strong reflector associated with the base of the near-surface with its multiple. (b) The i-stats equivalent-medium velocity field for the near-surface derived from the semblance picks from the CVM volume, (c) prestack depth migration using the velocity field in (b) with the common-image-point (CIP) gather at location B with maximum offset 1250 m, (d) the same depth image as in (c) with the picked depth horizon that represents the interface between the near-surface and the subsurface, and (e) the same velocity field as in (b) with the depth horizon picked from the depth image in (d). FD: floating datum that is a smoothed form of the topography and ID: intermediate datum.

reflector at the base of the near-surface to create the near-surface rms velocity field. Note that the reflector associated with the base of the near-surface is sufficiently strong to give rise to a prominent multiple.

- 4) This laterally varying, but vertically invariant, rms velocity field actually is equivalent to the near-surface interval velocity field (Figure 8b).
- 5) Perform prestack depth migration (PSDM) of shot records using the near-surface interval velocity field to obtain a shallow seismic image of the near-surface (Figure 8c). Check the flatness of the reflector on common-image-point (CIP) gathers

to verify the accuracy of the interval velocity field used for PSDM (Reshef, 1997).

- 6) Pick the depth horizon associated with the base of the near-surface from the shallow seismic image in depth (Figure 8d).
- 7) Combine the depth horizon with the interval velocity field to create the near-surface equivalent-medium model for statics corrections (Figure 8e).

Figure 9a shows the tomographic velocity–depth model for the near-surface derived from nonlinear traveltime inversion (Zhang and Toksöz, 1998) applied to first-arrival times picked

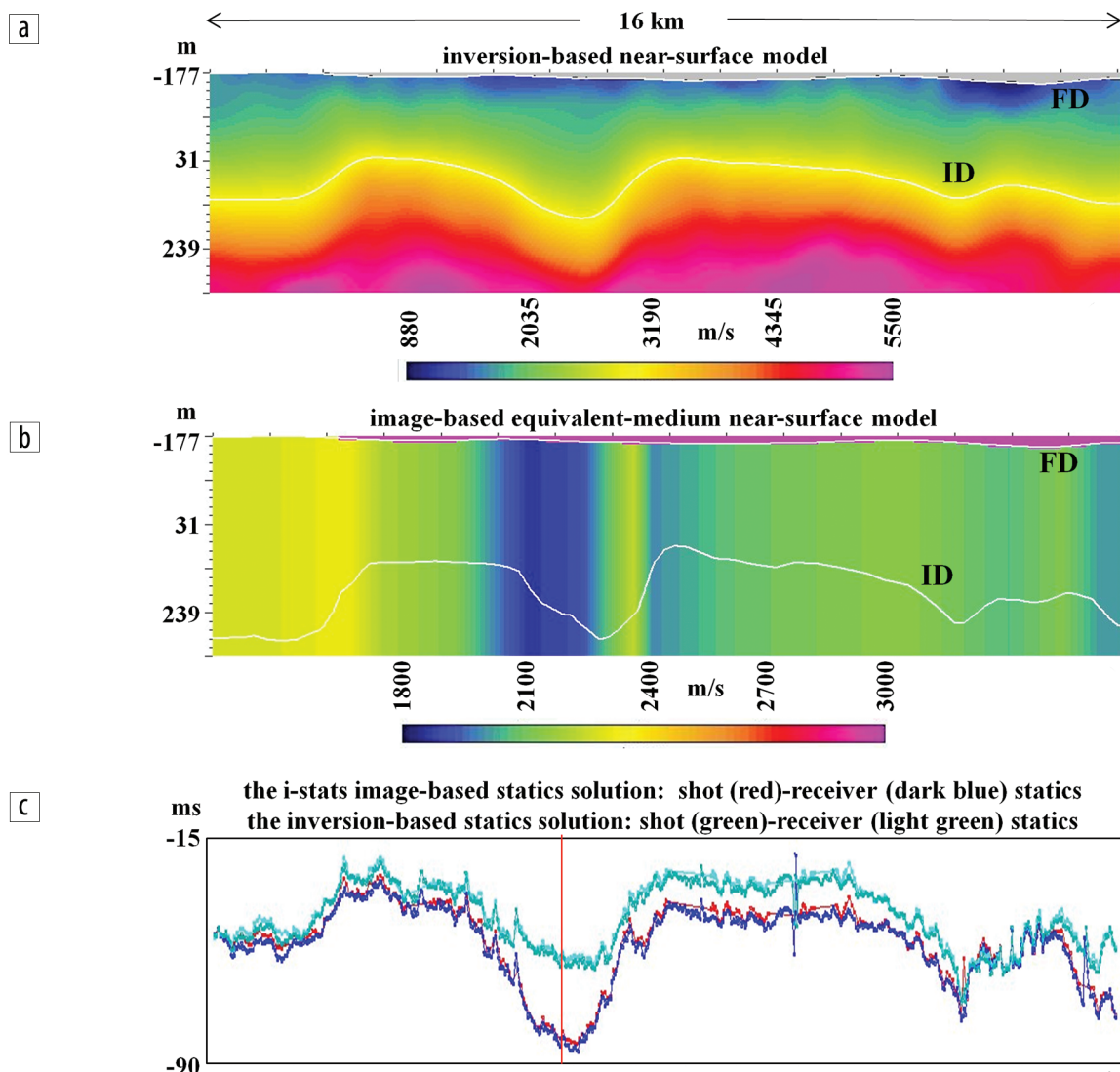


Figure 9. (a) The tomographic velocity-depth model for the near-surface derived from travel time inversion applied to first-arrival times picked from the shot gathers, (b) the i-stats equivalent-medium velocity-depth model for the near-surface as in Figure 8e, and (c) the shot-receiver statics calculated using the tomographic velocity-depth model in (a) and the i-stats equivalent-medium model in (b) combined with residual statics corrections for each case. FD: floating datum that is a smoothed form of the topography and ID: intermediate datum. Note that the long-wavelength solutions from the two methods depart significantly in the vicinity of the red vertical bar — corresponding to the collapse zone associated with the salt-filled karstic formation within the near-surface

from the shot gathers. Figure 9b shows the i-stats equivalent-medium velocity-depth model for the near-surface as in Figure 8e. Figure 9c shows the shot-receiver statics calculated using the tomographic inversion-based velocity-depth model (Figure 9a) and the i-stats equivalent-medium model (Figure 9b), combined with residual statics corrections for each case. Note that the long-wavelength solutions from the two methods depart significantly in the vicinity of the vertical red bar in Figure 9c — corresponding to the collapse zone associated with the salt-filled karstic formation within the near-surface. Traveltime inversion may not have completely resolved the velocity variations associated with the heterogeneity in the near-surface.

For an unbiased evaluation of statics corrections, we shall compare CVS panels with elevation statics, inversion-based statics, and image-based statics. Any subsequent processing, such as stacking and migration of data with different statics application would require different velocities; this would then make it difficult

to judge whether the differences are caused by different statics or different velocities. Figure 10a shows a CVS panel with a velocity optimum for the subsurface as in Figure 7b with elevation statics applied to lower the shots and receivers from topography to a floating datum followed by residual statics corrections, but without any long-wavelength statics corrections applied. Figure 10b shows a CVS panel with a velocity optimum for the subsurface with the application of long-wavelength shot-receiver statics calculated from the tomographic inversion-based solution as shown in Figure 9c followed by residual statics corrections. Finally, Figure 10c shows a CVS panel with a velocity optimum for the subsurface with the application of long-wavelength shot-receiver statics calculated from the i-stats image-based solution as shown in Figure 9c followed by residual statics corrections.

Irrespective of the method for near-surface modeling (Figure 1), the objective with long-wavelength statics corrections is to remove the deleterious effect of the near-surface anomaly on

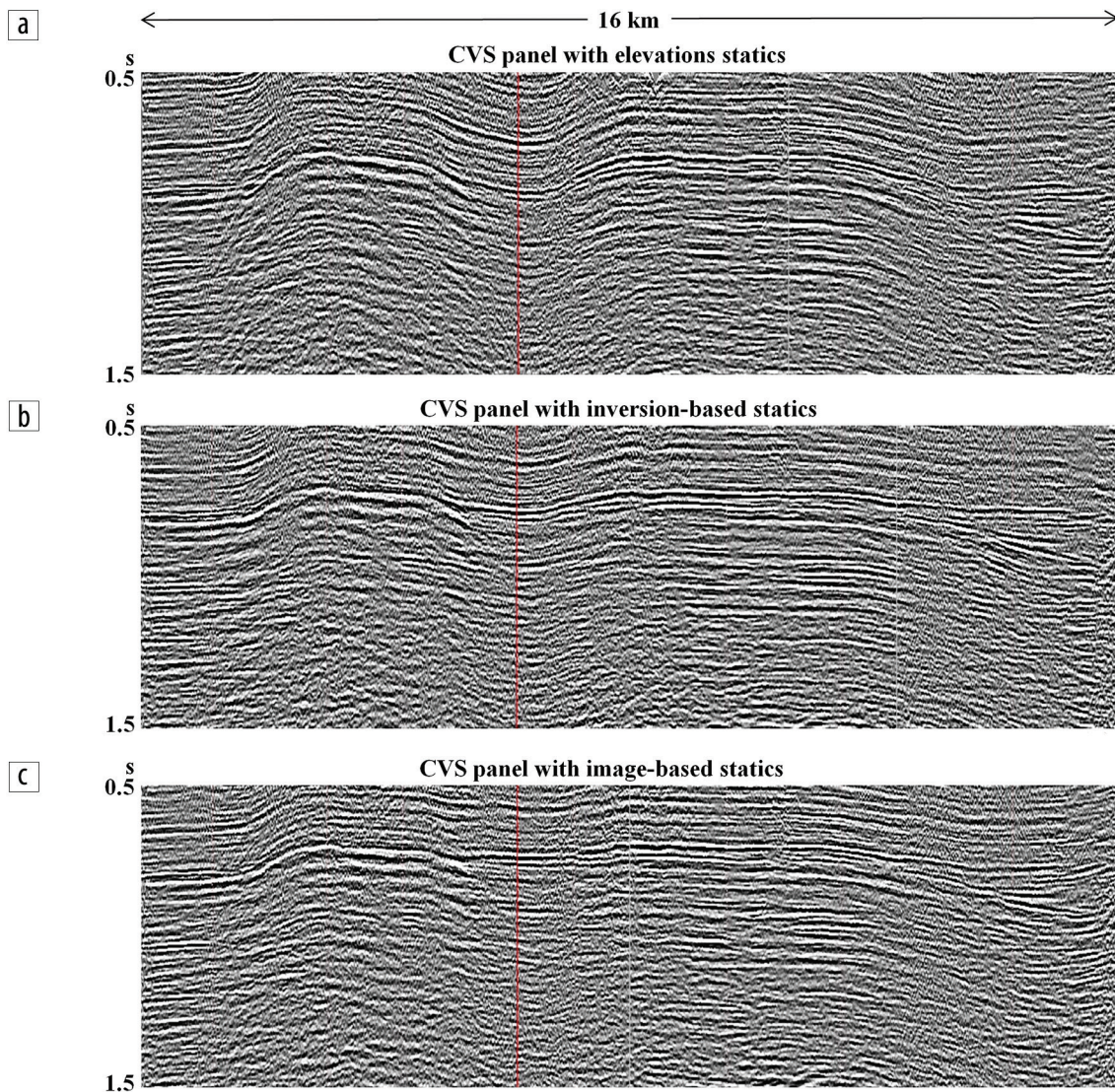


Figure 10. (a) A CVS panel with a velocity optimum for the subsurface as in Figure 7b with elevation statics applied to lower the shots and receivers from topography to a floating datum followed by residual statics corrections, (b) a CVS panel with a velocity optimum for the subsurface with the application of shot-receiver statics from the tomographic solution as shown in Figure 9c followed by residual statics corrections, and (c) a CVS panel with a velocity optimum for the subsurface with the application of shot-receiver statics from the i-stats solution as shown in Figure 9c followed by residual statics corrections.

reflection traveltimes as manifested by the CVS panel shown in Figure 10a. Subsequent to the long-wavelength statics estimation, irrespective of the method used, short-wavelength residual statics estimation must follow (Yilmaz, 2001). Since the ultimate deliverables from the near-surface modeling are shot-receiver statics, not the near-surface model itself, which should be treated as an intermediate product, then, the image-based equivalent-medium modeling is just as valid as any other method for near-surface corrections. Moreover, more than any other method, the equivalent-medium model conforms to the vertical-ray assumption underlying statics corrections.

Conclusions

I have demonstrated the new i-stats workflow to resolve the near-surface anomaly associated with salt-filled karstics formation. Although I presented a 2-D case study, the new i-stats workflow described in this paper also is readily applicable to 3-D land

seismic data. The i-stats method is applicable to correcting for near-surface anomalies associated with sand dunes, shallow anhydrites and salt bodies, shallow basalt layer, karstic formation, glacial tills, and permafrost.

The i-stats method is an image-based equivalent-medium near-surface modeling method. It does not require first-break picking as for traveltime tomography, does not require source wavelet estimation as for waveform inversion, does not fail velocity inversions as in traveltime tomography, does not suffer from velocity-depth ambiguity, does not require data modeling (traveltime or wavefield) as for any inversion method, and does not exhaust computational resources as in waveform and joint inversions. In contrast with tedious first-break picking in traveltime tomography, the i-stats method is based on event and semblance picking — interpretively appealing to the practicing geophysicist. In contrast with the yet-to-be-resolved practical aspects of waveform inversion and joint-inversion methods, the intuitively appealing image-based

i-stats method is extremely robust and efficient for modeling of near-surface anomalies. **LE**

Acknowledgments

I sincerely thank Paradigm Geophysical for providing the field data associated with the case study presented. I also thank Alexander Korolev and Evgeny Korolev of PetroTrace Services for discussions on the nature of the near-surface anomaly associated with the data used in the case study. I also thank the companies, who requested to be anonymous, for the field data cases shown in Figures 2–6.

Corresponding author: oz@anatoliangeo.com

References

- Abubakar, A., G. Gao, T. M. Habashy, and J. Liu, 2012, Joint inversion approaches for geophysical electromagnetic and elastic full-waveform data: *Inverse Problems*, **28**, no. 5, 19pp, <http://dx.doi.org/10.1088/0266-5611/28/5/055016>.
- Colombo, D., D. Rovetta, E. S. Curiel, R. E. Ley, W. Wang, and C. Liang, 2013, 3D seismic-gravity simultaneous joint inversion for near surface velocity estimation, 75th Conference & Exhibition, EAGE, Extended Abstracts, <http://dx.doi.org/10.3997/2214-4609.20130006>.
- Gallardo, L. A., and M. A. Meju, 2004, Joint two-dimensional DC resistivity and seismic travel time inversion with cross-gradients constraints: *Journal of Geophysical Research*, **109**, B3, B03311, <http://dx.doi.org/10.1029/2003JB002716>.
- Liu, Z., and J. Zhang, 2015, Joint traveltime and waveform envelope inversion for near-surface imaging: 85th Annual International Meeting, SEG, Expanded Abstracts, 1154–1158, <http://dx.doi.org/10.1190/segam2015-5863259.1>.
- Liu, Z., and J. Zhang, 2014, Pseudo 2D elastic full waveform inversion for near surface imaging: 84th Annual International Meeting, SEG, Expanded Abstracts, 1017–1021, <http://dx.doi.org/10.1190/segam2014-1059.1>.
- Marquis, G., W. Wang, and J. Ogunbo, 2016, 3D near-surface velocity modeling building by joint seismic-airborne EM inversion: 86th Annual International Meeting, SEG, Expanded Abstracts, 922–926, <http://dx.doi.org/10.1190/segam2016-13959497.1>.
- Ogunbo, J. N., and J. Zhang, 2014, Joint seismic traveltime and TEM inversion for near surface imaging: 84th Annual International Meeting, SEG, Expanded Abstracts, 2104–2108, <http://dx.doi.org/10.1190/segam2014-1056.1>.
- Reshef, M., 1997, The use of 3D prestack depth imaging to estimate layer velocities and reflector positions: *Geophysics*, **62**, no. 1, 206–210, <http://dx.doi.org/10.1190/1.1444120>.
- Yilmaz, O., 2001, Seismic data analysis: Processing, inversion, and interpretation of seismic data: Society of Exploration Geophysicists, <http://dx.doi.org/10.1190/1.9781560801580>.
- Yilmaz, O., 2013, An image-based effective-medium modeling of near-surface anomalies: *The Leading Edge*, **32**, no. 4, 394–401, <http://dx.doi.org/10.1190/tle32040394.1>.
- Yilmaz, O., 2015, Engineering seismology with applications to geotechnical engineering: Society of Exploration Geophysicists, <http://dx.doi.org/10.1190/1.9781560803300>.
- Zhang, J., and M. N. Toksöz, 1998, Nonlinear refraction traveltime tomography: *Geophysics*, **63**, no. 5, 1726–1737, <http://dx.doi.org/10.1190/1.1444468>.
- Zhang, J., and F. D. Morgan, 1997, Joint seismic and electrical tomography, Proceedings, SAGEEP 1997, Reno, Nevada, Environmental and Engineering Geophysical Society, 391–396.
- Zhang, J., and J. Chen, 2014, Joint seismic traveltime and waveform inversion for near surface imaging: 84th Annual International Meeting, SEG, Expanded Abstracts, 934–937, <http://dx.doi.org/10.1190/segam2014-1501.1>.
- Zhou, D., W. Wang, J. Zhang, and D. O'Connell, 2014, 3D joint inversion of seismic traveltime and gravity data: A case study: 84th Annual International Meeting, SEG, Expanded Abstracts, 3148–3152, <http://dx.doi.org/10.1190/segam2014-1556.1>.
- Zhou, X., D. P. Sixta, and B. G. Angstman, 1992, Tomostatics: Turning-ray tomography and statics corrections: *The Leading Edge*, **11**, no. 12, 15–23, <http://dx.doi.org/10.1190/1.1436864>.